ISSN: 2230-9926

Available online at http://www.journalijdr.com

IJDR

International Journal of Development Research
Vol. 11, Issue, 11, pp. 52213-52220, November, 2021
https://doi.org/10.37118/ijdr.23417.11.2021

RESEARCH ARTICLE OPEN ACCESS

NEW ANALYTICAL APPROACH TO ESTIMATE THE ELECTROMAGNETIC SPECTRUM ORIGINATED FROM DEVICES SUBMITTED TO HIGH VOLTAGES

Galba Falcão Aragão[1,*], Glauco Fontgalland[2], Humberto Dionísio de Andrade[3]

[1]Instituto Federal do Rio Grande do Norte - IFRN – Campus Parelhas, Parelhas, RN, Brasil; [2]Universidade Federal de Campina Grande – UFCG, CIEE – DEE, Campina Grande, PB, Brasil; [3]Universidade Federal Rural do Semi-Árido – UFERSA, DET, Mossoró, RN, Brasil

ARTICLE INFO

Article History:

Received 20th August, 2021
Received in revised form
10th September, 2021
Accepted 14th October, 2021
Published online 30th November, 2021

Key Words:

Corona Effect, EMI,
Electrostatic Source,
Electromagnetic Spectrum,
HV Electric Field.

Corresponding author:
Galba Falcão Aragão

ABSTRACT

This paper presents a simplified physical model and an analytical equation to estimate the frequency range of the radiated spectrum from an ionized region using computational simulation. This phenomenon is frequently caused by the corona effect generated from high voltages sources. Mostly not seem, this ionization can damage over time the device and the radiated frequencies can cause electromagnetic interference (EMI). Based on particle radiation and the momentum equation, the velocity and frequency equations for accelerated charges in an electric field are presented. The proposed model presents compatible results according to the results widely found in the literature, from kHz frequencies to infrared and ultraviolet ranges. The model also explains why the corona effect spectrum for slowly changing electric fields is limited to the ultraviolet range and why rapidly changing fields can emit X-ray signals. The results can be used to guide in the evaluation of devices submitted to high voltage (HV) as well as to contribute to the development of devices that use HV electric fields to generate high frequencies, such as X-ray sources, and to research on harvest energy systems, corona discharges industrial processes, among others.

Citation: ***Galba Falcão Aragão, Glauco Fontgalland, Humberto Dionísio de Andrade.*** "New analytical approach to estimate the electromagnetic spectrum originated from devices submitted to high voltages", *International Journal of Development Research*, 11, (11), 52213-52220.

INTRODUCTION

In the early 20th century, PEEK (1911, 1912) investigated that a loss occurs by dissipation of power into the air in alternating-current transmission lines at very high voltages and reported that this is accompanied by luminosity of the air surrounding the line conductor - the so-called corona. To LOEB (1965), the expression corona is used to describe the general class of luminous phenomena appearing associated with the current jump to some microamperes at the highly stressed electrode preceding the ultimate spark breakdown of the gap. According to GIAO & JORDAN (1968), corona discharges attract attention in power transmission engineering because of the breakdown phenomena and the mostly undesirable effects on insulation and because they produce radio noise and power loss. On the other hand, corona discharges are applied in many useful industrial processes. According to these authors, three conditions must be satisfied to initiate a corona discharge:

- Field intensity should be high enough,
- The degree of field nonuniformity should be high enough,
- Free electrons should be available in the overstressed field region.

As is already known a gas can be considered as an almost perfect insulator at normal state. However, when a high voltage is applied between two electrodes immersed in a gaseous medium, the gas can become a conductor (by ionization) and the dielectric breakdown can occur (NAIDU & KAMARAJU, 1997; DATSIOS & MIKROPOULOS, 2016).

In this process, the air can be ionized mainly by photoionization and collision (NAIDU & KAMARAJU, 1997), and detailed explanation of the air ionization process is presented in CHACHEREAU & PANCHESHNYI (2014). The air region where ionization processes occur is called the region of space charges. McMILLAN (1932) and LIM *et al.* (2019) present theories of formation of the regions of space charges and the corona effect in devices subjected to high alternating voltage (AC). In the ionization process, there is a delay between the discharge voltage and the discharge current, named time-lag (OKANO, 2013). The use of voltage impulses shorter than the time-lag allows to reach very high discharges voltages and, therefore, obtain electric fields greater than the breakdown limit (3 MV/m), under atmospheric conditions. X-ray emission has been detected occasionally during the streamer-corona propagation in a wire-plate corona reactor open to ambient air (NGUYEN *et al.*, 2009) using an impulse generator superimposed on a 20 kV DC bias. Because of the short pulse duration regarding the primary streamer transit time, no total gap breakdown occurred. Electrical energy in the corona discharges is transformed into other forms of energy: light, sound, electromagnetic energy, etc. However, the main part of energy is lost in the collisions of electrons and ions with neutral gas molecules. In other words, the main effect of corona loss is the gas heating (GIAO & JORDAN, 1968). Several measurement systems have been developed using the corona effect to identify the conservation status of elements subjected to high voltage (HV). The corona effect is detected indirectly based on measurement of conducted current (CHUN *et al.*, 2001), ultraviolet radiation (PINNANGUDI *et al.*, 2002; PINNANGUDI *et al.*, 2005), thermographic cameras, sound, and ultrasound (VAHIDI *et al.*, 2003), and measurement of the radiated electromagnetic spectrum (FONTGALLAND *et al.*, 2004; ROCHA & FONTGALLAND, 2014).

In his study on the radio interference (RI) caused by air ionization and corona effect in high alternating voltages, McMILLAN (1932) attributes the RI to small ionizations or corona discharges due to the high electric field. According to ZAAZOU *et al.* (1964), RI can also be produced by elements subject to high direct voltage. ADAMS (1956) proposed a method to calculate the RI Level from transmission line using laboratory results on conductor samples and knowledge of the geometry of the line. From the above, HV devices can radiate EM waves (SARATHI & UMAMAHESWARI, 2013). And these EM waves can cover the spectrum of radio waves, ranging from the infrared range to the ultraviolet range. And in special conditions, reaching the X-ray range (NGUYEN *et al.*, 2009). Several studies have been carried out to assess the state of electrical components subject to high electric fields based on changes in their electromagnetic emissions (FONTGALLAND *et al.*, 2004; ROCHA & FONTGALLAND, 2014; MOURA *et al.*, 2014; FONTGALLAND & PEDRO, 2015; SARATHI *et al.*, 2008). However, there is not much information about the spectral band emitted, which can be used to select the sensor's frequency band and the origin of electromagnetic interference (EMI) source as well. When evaluating the problem of EMI emissions originated from devices submitted to HV, it was realized that the emissions occur because of the ionization of the air and by the movement of charges in the region. Therefore, the ionization effect can be obtained from electrostatic sources, as demonstrated in ARAGÃO *et al.* (2017). These important results and the lack of an expression to estimate the frequency range of the EMI field have encouraged our study on the determination of the spectrum radiated by the corona effect using analytical formulation. The use of an electrostatic source, such as the Wimshurst electrostatic machine, greatly simplified the experiments and the experimental results can accurately be applied to HV components without lost of generality (ADAMS, 1956). This paper presents a simplified model that allows to achieve an equation for radiated spectral range estimation generated by ionization and the corona effect. The equation is based on the intensity of the electric field and the distance that the electron can take between collisions and its acceleration.

MATERIALS AND METHODS

The following steps were taken to solve the problem of determining the frequency range radiated by corona effect in transmission line elements subjected to high voltage, mainly insulators:

- Elaboration of a simplified physical model.
- Development of the model equation.
- Model simulation using routines developed for MATLAB® software.

RESULTS

Particle radiation: Electromagnetic emissions from a device subjected to high electric field are related to the air ionization (GIAO & JORDAN, 1968; McMILLAN, 1932; ZAAZOU *et al.*, 1964, ADAMS, 1956). Therefore, the frequency range emitted by this type of source are proportional to the variation in the electrical charges speed in the region of space charges. This variation, in turn, depends on the distance between collisions and the intensity of the electric field. Based on antenna theory (BALANIS, 2005), for an electromagnetic signal to radiate, there must be a variation in the conductor current. In the region of space charges subjected to HV, the charges are basically electrons, positive ions, and negative ions. This consideration is in line with ADAMS (1956), which states that this movement of charge, both positive and negative, constitutes an electric current, $I = dQ/dt$. For simplicity, only electrons will be considered.

The proposed model: The model is based in two charged electrodes (A and B). The electrode A is charged with $Q_A = +Q$ and B is charged with $Q_B = -Q$ (where $|Q_A| = |Q_B| = |Q|$). Considering that only a single electron subjected to the electric field between the electrodes, with rest mass m_0 departs from the proximity of the negative electrode and it is accelerated towards the positive electrode (Fig. 1) in a straight line. According to GRIFFITHS (2013) when charges accelerate, their fields can transport energy irreversibly out to infinity – the electromagnetic radiation.

The electron undergoes several inelastic collisions with other atoms or ions and its energy is transferred to them. After each collision, the electron's velocity is considered to drop to zero. Here it should be noted that, by the equation of momentum $p = m_0 v/\sqrt{1 - v^2/c^2}$ (DE BROGLIE, 1924), where c is the speed of light, if the velocity v drops to zero, the momentum will be zero, and this model will be invalidated. But, according to LANDAU & LIFSHITZ (1975), in relativistic mechanics, the energy (ε) of a free particle does not go to zero for $v = 0$. This can be seen in Eq. (1):

$$\varepsilon = \frac{m_0 c^2}{\sqrt{1-\frac{v^2}{c^2}}} = m_0 c^2|_{v=0} \quad (1)$$

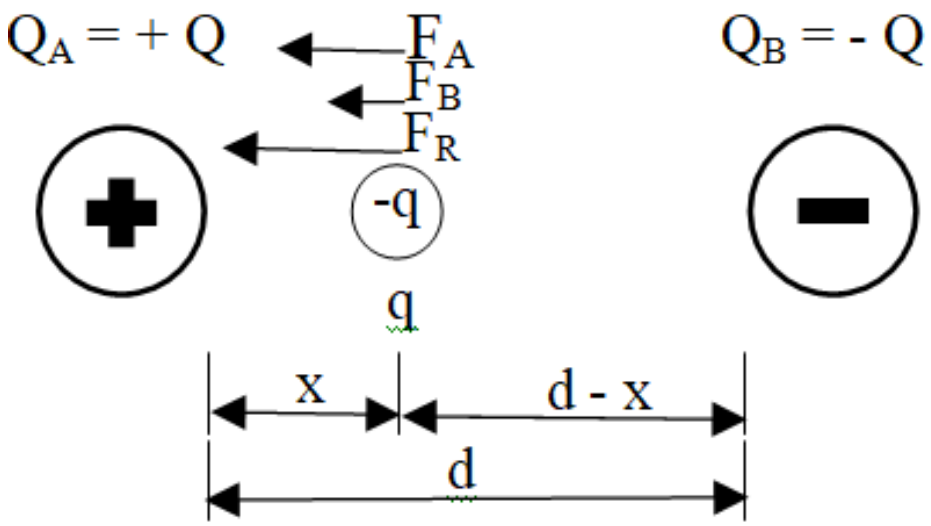

Fig. 1. Representation of forces acting on an electrical charge between two electrodes

As the momentum can be related to the energy by $p = \varepsilon/c$, it is verified that the momentum will not be 0 ($p = m_0c$). In this model, the electron does not recombine during its journey, and, after each collision, the electron resumes its movement since it remains subjected to the electric field. The acceleration of the electron, in the region of space charges, is responsible for electromagnetic emissions. This statement seems to violate the energy and momentum conservation laws, however, as will be seen, when the electron is accelerated, an electromagnetic field proportional to its acceleration appears in the opposite direction, causing its resulting acceleration to decrease with increasing velocity. And this deceleration effect is responsible for the electromagnetic emissions of accelerated charges and is in accordance with the energy and momentum conservation laws.

The model equation: To define the equation that can indicate the electromagnetic spectrum radiated by the proposed model, the momentum equation will be used as a starting point

$$p = \frac{m_0 v}{\sqrt{1-\frac{v^2}{c^2}}}. \quad (2)$$

The wavelength of a particle can be related to its momentum by the Eq. (3), as

$$\lambda = \frac{h}{p}, \quad (3)$$

where h is the Planck constant. The wavelength can also be related to the particle oscillation frequency in free space by (in media, refractive index must be included)

$$\lambda = \frac{c}{f}, \quad (4)$$

where f is the frequency. Combining Eq. (2), (3) and (4), is obtained

$$f = \frac{c m_0 v}{h\sqrt{1-\frac{v^2}{c^2}}} \quad (5)$$

The frequency determined in Eq. (5) varies if the particle v varies, by the Lorentz factor.

The Electric Field Behavior

Since the frequency of the applied voltage is relatively low, the distribution of the electric field can be calculated by the methods employed to electrostatic fields (ADAMS, 1956). The problem in determining the particle acceleration can be modeled by an electric charge (electron, $-q$) subjected to an electric field between two electrodes as shown in Fig. 1.

Coulomb's Law shows that electrical force can be given by

$$F_R = F_A + F_B = k|Q||q|\left(\frac{1}{x^2} + \frac{1}{(d-x)^2}\right). \quad (6)$$

The resulting electric field can be obtained from

$$E = \frac{F_R}{|q|}, \quad (7)$$

where F_R is the resultant force that the charge q undergoes when placed between the electrodes with charges Q_A and Q_B in relation to their position.

Charge acceleration: The particle acceleration, considering the variation of mass with velocity, is given by Eq. (8), which corresponds to the *x* direction. In this study, the displacement was considered only in the *x* direction, according to the proposed model. The applied force corresponds to the electrical force that the electron is subjected to, which is given by

$$a_x = \frac{F_x}{m_0}\left(1 - \frac{v^2}{c^2}\right)^{3/2} \tag{8}$$

From Eq. (7), the force in the *x* direction can be represented by $F_x = |q|E_x$, therefore, the acceleration as a function of the electric field can be written as

$$a_x = \frac{|q|E_x}{m_0}\left(1 - \frac{v^2}{c^2}\right)^{3/2}. \tag{9}$$

An important interpretation of the result presented in Eq. (9) is that the acceleration decreases as the particle speed increase. And this deceleration effect may explain why accelerated charges are able to radiate electromagnetic emissions without violating energy and momentum conservation laws.

Charge velocity: To determine the velocity of the particle, an infinitesimal element of length, ds_0, was considered, which corresponds to the distance traveled by a low-speed particle. The electric field will be considered constant in this element of length and, therefore, we can simplify the movement of the particle to the uniformly accelerated rectilinear movement (UARM). Because of space contraction at high speeds, the infinitesimal element of length, *ds*, can be determined by Eq. (10)

$$ds = \sqrt{1 - \frac{v^2}{c^2}}\, ds_0\,. \tag{10}$$

Hence, the Torricelli equation (Eq. (11)) is used to determine the velocity of particle in each element of length *ds,*

$$v_{(s)} = \sqrt{{v_0}^2 + 2\,ads}\,. \tag{11}$$

Therefore, replacing Eq. (9) and Eq. (10) in Eq. (11), we have

$$v_{(s)} = \sqrt{{v_0}^2 + 2\,\frac{|q|E_x}{m_0}\left(1 - \frac{v^2}{c^2}\right)^2\, ds_0} \tag{12}$$

Eq. (12) shows that the particle velocity increases with: the distance between collisions increases; the increase of the element electrical charge; the increase of the electric field.

Frequency emitted by an accelerated charge Substituting Eq. (12) in Eq. (5), we obtain:

$$f = \frac{cm_0}{h\sqrt{1-\frac{v^2}{c^2}}}\sqrt{{v_0}^2 + 2\,\frac{|q|E_x}{m_0}\left(1 - \frac{v^2}{c^2}\right)^2\, ds_0}. \tag{13}$$

In Eq. (13) it can be observed that the frequency increases with the increase of the particle velocity and with its mass. It must be pointed out here that Eq. (13) governs the behavior of the electron under BC considered in our model.

SIMULATED RESULTS

Computational routines were developed to implement the BC to the proposed equations providing simulated results and their graphical representations. These simulations were performed in MATLAB® to evaluate the behavior of the particle velocity (Eq. (12)) and the radiated frequency (Eq. (13)). Histograms of the occurrences of radiated frequencies were constructed to represent the radiated spectrum. The profile of the resulting electric force was calculated from Eq. (6), where was considered: $|Q|$ = 1 pC, $|q|$ = 1.6021917x10^{-19} C, and d = 3 cm. These parameters correspond approximately to the configuration presented by a Wimshurst electrostatic machine with its electrodes separated by 3 cm. The resulting electric field was calculated using Eq. (7) (Fig. 2). As expected, the electric field tends to have very high values in the vicinity of the electrodes, consequently, very high frequencies. However, the dielectric strength constant of the air must be considered, and the electric field has its maximum value limited to 3 MV/m in the vicinity of the electrodes.

For simulating the collisions occurred by the electron during the path between the electrodes, the interval between collision can be estimated by considering the Van der Waals radii for nitrogen and oxygen (Table 1), since these elements correspond to 78% and 21% of the atmosphere composition, respectively. This approach to the composition of the atmosphere is in accordance with CHACHEREAU & PANCHESHNYI (2014). For proof of concept (PoC), we assume that the minimum distance between a collision is 150 *p*m, which corresponds approximately to the Van der Waals radii for nitrogen and oxygen. It was added to the minimum distance interval ten times its length (10 ×150 *p*m) to define the longest distance between a collision, which corresponds to 1,650 *p*m. Thus, the distances between the collisions were calculated using a normal distribution with an average of 900 *p*m and standard deviation of σ = 300 *p*m, which should happen in the interval between 150 *p*m and 1,650 *p*m. The choice of collision distances was hypothetical. Air density is related to the longest collision interval. If the air density increases, the collision interval decreases, and the maximum frequencies decrease. If the air density decreases, higher frequencies can be obtained. Fig. 3 shows

the simulated results for the electron velocity (Eq. (12)) and for the radiated frequency (Eq. (13)), in a linear scale, considering that a single collision occurs at 900 *p*m. Fig. 3a shows that the particle starts to move at a *v = 0 m/s* (initial condition).

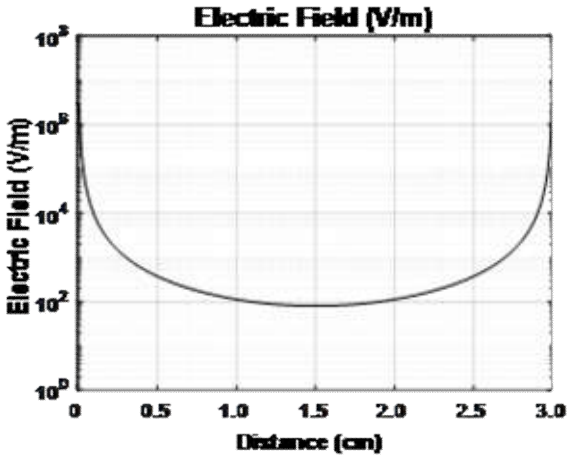

Fig. 2. Simulated results for electric field between two electrodes 3 cm apart

Table 1 – Radii of nitrogen and oxigen.

Element	AtomicRadius (*p*m)	CovalentRadius (*p*m)	Van der Waals Radius (*p*m)
Nitrogen (N_2)	65	75	155
Oxigen (O_2)	60	73	152

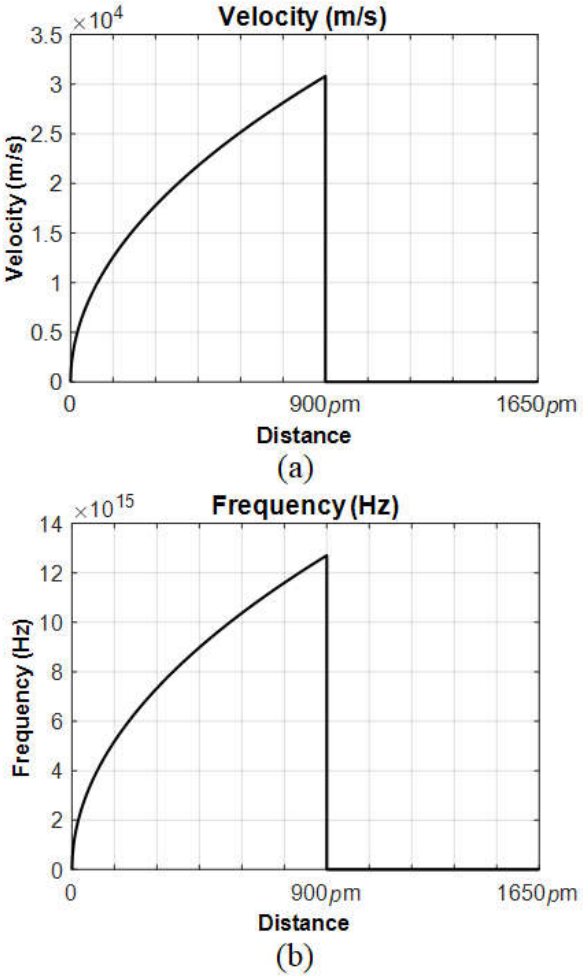

Fig. 3. Simulated results for (a) velocity of electron and (b) radiated frequency considering the electric field limited to 3 MV/m for a single collision at 900 *p*m, in the interval between 0 *p*m and 1,650 *p*m

As the traveled distance increases the velocity grows and the acceleration reduces. The phenomenon continues until the collision occurs and the velocity drops back to *0 m/s*. The radiated frequency variation has the same characteristic to the velocity, as can be seen in Fig. 3b. The graphs shown in Figs. 4, and 5 represent the solutions of Eq. (12) (for velocity) and Eq. (13) (for frequency). Three frames taken into the space variation of 30 nm located around the beginning (0 cm + 30 nm), middle (1.5 cm ±15 nm), and the end (3 cm – 30 nm) of the path between the electrodes

were simulated for the electric field curve in Figure 2. The first and third frames show very similar results, as the electric field is limited to 3 MV/m. The third frame is not shown. As can be seen, 30 nm spatial variation was enough to represent the number of collisions (approximately 30 collisions). This space variation was further divided into $1x10^6$ linear parts, which represent the infinitesimal elements in length ($ds_0 = 3x10^{-14}$ m). The plots are presented in logarithmic scale and show the velocities and frequencies at the second interaction interval. For the electron, the infinitesimal element of length, ds_0, is large enough to cause great acceleration. This effect hides lower velocities and frequencies in Figs. 4, and 5. Using linear scale plots, these smaller values become more evident (Fig. 3). Therefore, there is no restriction on the use of Eqs. (12) and (13). Fig. 4a shows that the initial variation in speed of electron is very intense.

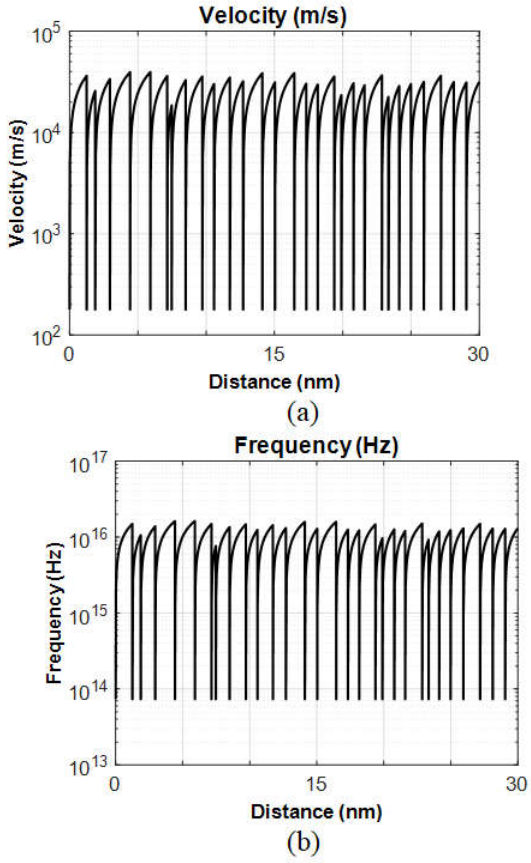

Fig. 4. Simulated results for (a) velocity of electron and (b) radiated frequency considering the electric field limited to 3 MV/m for distances between 0 nm and 30 nm

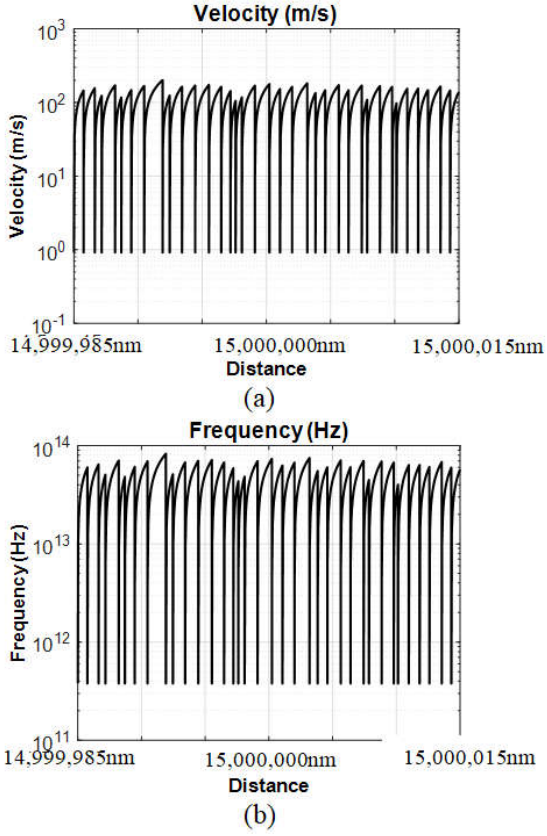

Fig. 5. Simulated results for (a) velocity of electron and (b) radiated frequency considering the electric field limited to 3 MV/m for the 1.5 cm +/- 15 nm interval

This intense velocity variation causes the frequency (Fig. 4b) to vary very quickly. This variation decreases when it tends to its maximum value because of the Lorentz factor. It is also observed that the maximum frequency emitted by the charge in each path depends on the electric field. In the case of free space, where the dielectric strength is 3 MV/m, the maximum frequencies will be in the ultraviolet range (10^{16} Hz). These emissions will occur near the electrodes (Figs. 4) since the electric field is stronger in these surroundings. Due to the variation of the electric field with the distance, the maximum frequencies fall rapidly to values in the infrared region ($f < 10^{14}$ Hz) (Fig. 5).

It can be seen from Eq. (13) that the frequency varies from values close to zero to values in the order of 10^{16} Hz. Eq. (13) was calculated to demonstrate the frequency range emitted throughout the path between the electrodes. The occurrences of each frequency were counted generating the histogram shown in Fig. 6. From the comments above, it is highlighted here that both scales are logarithmic. To perform this calculation, 1,000 points, logarithmically spaced, were used in the interval between each collision (approximately 33 million collisions between the electrodes were considered). The starting distance range is $ds_o = 1x10^{-34}$ m. The use of a linear scale would better represent the emissions profile, however, the limitation of the processing capacity of the used system did not allow its use. Fig. 6 shows the full spectrum, where the maximum frequencies are limited by the maximum electric field (3 MV/m).

The same results were obtained with 100,000 points between collisions. The histogram was used to demonstrate that the frequencies are emitted in a wide range. Fig. 6 shows the presence of radiated frequencies from 10 kHz to 100 PHz. The electric field is more intense near the electrodes and decreases when moving away from them. We can remark also that the occurrence of frequencies higher than 100 THz decreases in relation to the others. The use of logarithmic scale to calculate the radiated frequencies produces the sawtooth shape-curve of the histogram, Fig. 6. This result is compatible with the spectrum proposed by ADAMS (1956). However, this reference does not present the frequency spectral range. The spectrum emitted by an element subjected to high voltage occurs during the ionization process of the medium and is influenced by the intensity of the electric field, the dielectric strength constant of the ionizable medium, and the distance between collisions of the charged particles in the region of space charges. To obtain higher frequencies, such as x-ray signals, the interval between collisions or the intensity of the electric field must be increased. The interval between collisions can be increased, decreasing the density of the air. HV pulses with duration less than the time-lag between discharge voltage and discharge current can be used to obtain electric fields greater than 3 MV/m in atmospheric conditions, as shown in NGUYEN *et al.* (2009). The spectrum emitted by an element subjected to high voltage occurs during the ionization process of the medium and is influenced by the intensity of the electric field, the dielectric strength constant of the ionizable medium, and the distance between collisions of the charged particles in the region of space charges. As the intensity of the electric field influences the velocity of particle, the

higher frequencies (UV) will be emitted at the places of greater intensity of the electric field, making the source of emission to be close to the surface responsible for the electric field or at the concentration points, as quoted by GIAO & JORDAN (1968).

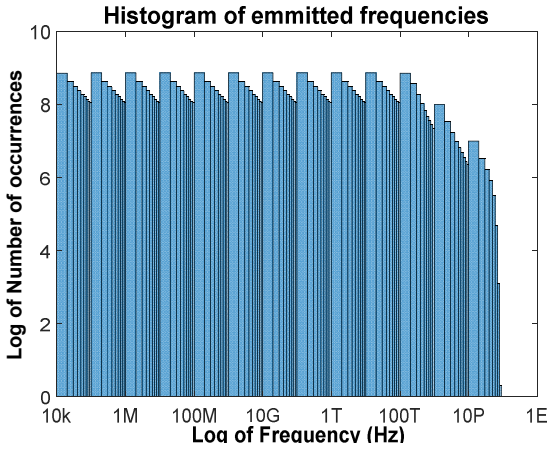

Fig. 6. Histogram representation of the radiated frequencies from 10 kHz up to 100 PHz (1x10^{17} Hz).

The developed equations and simulations showed that the radiated spectrum can start near to zero until very high frequencies, which is limited by the dielectric strength of the medium, and for the air in atmospheric conditions, it reaches ultraviolet range. The results obtained and the formulation presented demonstrate that the radiated spectrum is mainly due to the accelerated movement of electrons and an amount of emitted energy is available to be used.

CONCLUSION

The obtained results can make a valuable contribution to the study of air ionization and the corona effect. They contribute to the development of techniques for the electrical components' characterization subject to HV, as well as guide the development of devices that use electric fields to generate high frequencies. The proposed model for calculating the frequency spectrum generated by air ionization and the corona effect presents compatible results with the results widely found in the literature up to ultraviolet frequencies. The model also explains why the corona effect spectrum for slowly changing electric fields is limited to the ultraviolet range and why rapidly changing fields can emit X-ray signals. The presented model contribution goes beyond the characterization of the spectrum radiated by devices and may contribute to research on X-ray generation, generators in the terahertz range, harvest energy systems, ISM band applications, corona discharges industrial processes, among others.

Funding: This research did not receive any specific grant from funding agencies in the public, commercial, or not-for-profit sectors.

REFERENCES

Adams, G. E. (1956) *The Calculation of the Radio Interference Level of Transmission Lines Caused by Corona Discharges* [includes discussion]. Transactions of the American Institute of Electrical Engineers. Part III: Power Apparatus and Systems 75.3, pp. 411-419.

Aragão, G. F.; Fontgalland, G.; Andrade. H. D. (2017) *Measuring potential EMI fields from electrostatic sources*. 2017 IEEE International Symposium on Antennas and Propagation & USNC/URSI National Radio Science Meeting, San Diego, CA: pp. 2607-2608.

Balanis, C. A. (2005) *Antenna Theory: Analysis and Design,* 3rd Edition, John Wiley and Sons, New York.

Chachereau, A.; Pancheshnyi, S. (2014) *Calculation of the Effective Ionization Rate in Air by Considering Electron Detachment from Negative Ions*. IEEE Transactions on Plasma Science, 42(10), pp.3328-3338, 2014.

Chun, L.; Yuanfang, W.; Yixiong, N.; Munong, M.; Guofu, D.; Kecheng, L. (2001) *Investigation on characteristics of corona current to single insulator*. In Electrical Insulating Materials, (ISEIM 2001). Proceedings of 2001 International Symposium on (pp. 286-289). IEEE.

Datsios, Z.G.; Mikropoulos, P.N. (2016). *Modeling of lightning impulse behavior of long air gaps and insulators including predischarge current: implications on insulation coordination of overhead transmission lines and substations Lightning overvoltage performance of 110 kV air-insulated substation*, Electr. Power Syst. Res. 139, pp. 37–46.

de Broglie, L. -V. 1924 *Recherches sur la théorie des Quanta*. Physique [physics]. Migration - université en cours d'affectation, Français. tel-00006807.

Fontgalland, G.; Pedro, H. J. G. (2015) *Normality and Correlation Coefficient in Estimation of Insulators' Spectral Signature*. Signal Processing Letters, IEEE 22, no. 8: 1175-1179.

Fontgalland, G.; Vuong, T. P.; Bezerra, J. M. B.; Neri, M. G. G.; Baudrand, H.; Raveau, N. (2004) *Electromagnetic noise measured from glass insulator under discharge activity*. In 12° Colloque International de Compatibilité Electromagnétique, pp. 00-001.

Giao, T. N.; Jordan. J. B. (1968) *Modes of corona discharges in air*. IEEE transactions on power apparatus and systems 5, 1207-1215.

Griffiths, D. J. (2013). *Introduction to Electrodynamics*. 4th Edition, Pearson Education, Inc.

Landau, L. D.; Lifshitz, E. M. (1975) *The Classical Theory of Fields: Volume 2.* Butterworth-Heinemann.

Lim, D. Y.; Jee, S. W.; Bae, S.; Choi, Y.K. (2019) *Analysis of the influence of a conductive particle on the surface flashover characteristics of epoxy dielectric in atmospheric air*. Journal of Electrostatics 99, pp. 31-40.

Loeb, L. B. (1965). "Electrical coronas, their basic physical mechanisms." Univ of California Press.

McMillan F. O. (1932) *Radio interference from insulator corona*. Transactions of the American Institute of Electrical Engineers. 2, no. 51: 385-391.

Moura, E. P.; Albert, B. B.; Fontgalland, G. (2014) *Statistical classification of contamination in glass insulators by reading its spectrum*. International Journal of Applied Electromagnetics and Mechanics 45, no. 1-4: 589-595.

Naidu, M. S.; Kamaraju, V. (1997) *High Voltage Engeneering*, 2nd Edition, McGraw-Hill.

Nguyen, C. V. *et al.* (2009) *X-ray emission in streamer-corona plasma*. Journal of Physics D: Applied Physics 43.2, 025202.

Okano, D. (2013) *Time-lag properties of corona streamer discharges between impulse sphere and dc needle electrodes under atmospheric air conditions*. Review of Scientific Instruments 84.2, 024702.

Peek, F. W. (1911)*The law of corona and the dielectric strength of air*. Proceedings of the American Institute of Electrical Engineers 30.7: 1485-1561.

Peek, F. W. (1912) *The law of corona and dielectric strength of air—II*. Proceedings of the American Institute of Electrical Engineers 31.6 (1912): 1085-1126.

Pinnangudi, B. N.; Gorur, R. S.; Kroese, A. J. (2002) *Energy quantification of corona discharges on polymer insulators*. In Electrical Insulation and Dielectric Phenomena, Annual Report Conference on (pp. 315-318). IEEE.

Pinnangudi, B. N.; Gorur, R. S.; Kroese, A. J. (2005) *Quantification of corona discharges on nonceramic insulators*. IEEE Transactions on Dielectrics and Electrical Insulation, 12(3), pp.513-523.

Rocha, P. H. V.; Fontgalland, G. (2014) *Measuring the radiation bands of overhead power lines glass insulators*. In Antenna Measurements & Applications (CAMA), 2014 IEEE Conference on, pp. 1-3. IEEE.

Sarathi, R.; Reid, A. J.; Judd, M. D. (2008) *Partial discharge study in transformer oil due to particle movement under DC voltage using the UHF technique*. Electric Power Systems Research 78, no. 11, pp. 1819-1825.

Sarathi, R.; Umamaheswari. R. (2013) *Understanding the partial discharge activity generated due to particle movement in a composite insulation under AC voltages*. International Journal of Electrical Power & Energy Systems 48, pp. 1-9.

Vahidi, B.; Alborzi, M. J.; Aghaeinia, H.; Abedi, M. (2003) *Acoustic diagnoses of AC corona on the surfaces of insulators*. In Power Tech Conference Proceedings, IEEE Bologna (Vol. 2, pp. 5-pp). IEEE.

Zaazou, A.; Khalifa, M.; El-Debeiky, S. (1964) *Radio noise due to insulator corona*. Electrical Engineers, Proceedings of the Institution of, 111(5), pp.959-966.

****